Eur. Phys. J. D **42**, 235–241 (2007)
DOI: 10.1140/epjd/e2007-00030-0

THE EUROPEAN PHYSICAL JOURNAL D

Electron collisional excitation of argon-like Ni XI using the Breit-Pauli R-matrix method

Breit-Pauli R-matrix calculation for electron impact excitation of Ni^{10+}

N. Verma[a], A.K.S. Jha, and M. Mohan

Department of Physics and Astrophysics, Delhi University, Delhi 110007, India

Received 6 July 2006 / Received in final form 4 December 2006
Published online 14 February 2007 –

Abstract. Electron excitation collision strengths for the transitions from the ground state to the fine-structure levels of the $3s^2 3p^5 3d$ and $3s^2 3p^6 3d$ configurations in Ni XI are calculated using the Breit-Pauli R-matrix method. Configuration interaction wavefunctions have been used to represent the target states. The relativistic effects are incorporated in the Breit-Pauli approximation by including one-body mass correction, Darwin, and spin-orbit interaction terms in the scattering equations. Collision strengths are tabulated at selected energies in the range 10 to 75 Rydberg. Effective collision strengths are determined by integrating collision strengths by assuming a Maxwellian distribution of electron energies. The effective collision strengths are listed over a wide temperature range ($2 \times 10^4 - 1 \times 10^7$ K) applicable to astrophysical plasmas. Our results are the only collision strengths and effective collision strengths available for this ion. We believe that the data calculated in this work will be useful in solar, astrophysical and laser applications.

PACS. 34.80.Dp Atomic excitation and ionization by electron impact – 34.80.Kw Electron-ion scattering; excitation and ionization

1 Introduction

In recent years there has been great interest in the study of interactions of electrons and photons with positive ions, particularly with metallic impurities such as Ni, Fe, Cr, and Ti, because of their importance in fusion plasmas [1], and in astrophysical plasmas [2]. Nickel is an important impurity element in modern fusion research devices, especially in those where the vessel walls are constructed largely of high-nickel-content alloys (e.g., JET the Joint European Torus). Knowledge of atomic processes involving nickel ions is essential in order to understand and accurately model these plasmas. Nickel is the second most abundant transition element in the Sun after iron. Emission lines from ions of nickel have been identified in the ultraviolet (UV) and extreme ultraviolet (EUV) solar spectra [3–7]. Recently, Stellar parameters and element abundances of Ni have been derived for a sample of 18 F-K dwarfs of the young open cluster IC 4665 [8]. Raassen et al. [9] analyzed the high-resolution soft X-ray spectrum of the nearby F-type star Procyon in the wavelength range 5−175 Å and identified Ni XI emission lines at 78.73 Å and 148.36 Å. The Ni XI lines at 148.402, 78.744, and 77.393 Å have been observed in the spectrum of corona of Alpha Centauri by LETGS on board the Chandra [10]. Ni XI emission lines have also been observed by the Extreme Ultraviolet Explorer (EUVE) in the spectra of the K1V and G2V stars, which is very similar to the Sun [11]. Dere et al. [12] carried out an extensive study of potential electron density diagnostics for the high-temperature component ($>5 \times 10^5$ K) of solar flares and predicted that the nickel ions, corresponding to the iron ions, could also be useful for electron density diagnostics. Modelling of spectra and their interpretation require accurate rate coefficients or effective collision strengths [13]. Detailed electron-ion collision data are essential for understanding the behaviour of plasmas and for identifying electron impact excitation lines in various astronomical objects and enable the evaluation of electron densities [14], temperatures and abundances. Hence, there is an increasing demand for electron excitation data from many fields ranging from laser design, fusion reactor research and industrial plasma generation through to astrophysics. The effective collision strengths are needed over a wide temperature range to cover various astrophysical objects, where these ions can be present at temperatures far away from the temperature of formation in solar corona under the conditions of ionization equilibrium.

Much attention has been paid in the last years to the Ni XI ions in the solar corona, since they may account for many spectral lines of low ionization potential. Feldman et al. [15] identified a strong $3p^6 - 3p^5 3d$

[a] e-mail: verma_nupur123@rediffmail.com

transition of Ni XI at 148.5 Å with 9×10^2 counts per second in the far ultraviolet solar spectrum obtained by Hinteregger et al. [16]. There are many observations including Alexander et al. [17] and Gabriel et al. [18] for the transition from the $3p^5 3d\ ^1\mathrm{P}^\circ_1$ level to the ground state. A laboratory study of extreme-ultraviolet spectral lines by Wagner and House [19] provided empirical data on the $3p^5 3d$ configuration in Ni XI. Svensson et al. [20] ascribed three lines observed by Behring et al. [21] to the transitions from the $3p^5 3d\ ^3\mathrm{P}^\circ_{1,2}$ and $^3\mathrm{D}^\circ_1$ levels to the ground state on the basis of an isoelectronic extrapolation. Even-Zohar and Fraenkel [22] classified some Ni XI lines below 100 Å. An extended analysis of the forbidden transitions within the $3s^2 3p^5 3d$ configuration was made by Edlén and Smitt [23]. Sandlin and Tousey [24] observed solar coronal lines in ATM UV spectra and identified Ni XI transitions from the metastable levels in the $3p^5 3d$ excited configuration. Alexander et al. [25] observed two lines due to the transitions from the $3p^5 4s$ levels to the ground state. The transition array $3p^5 3d – 3p^5 4f$ in the region 81−94 Å was first identified by Fawcett et al. [26]. Ni XI lines from coronal spectra were checked by means of line intensity ratios by Magnant-Crifo [27] from observations obtained at the 1965 eclipse. Electron impact ionization cross sections were calculated in the distorted-wave approximation in the Ni isonuclear sequence, except Ni^{10+}, by Griffin and Pindzola [28] and were also measured by Wang et al. [29]. Cherkani et al. [30] measured absolute cross sections for electron impact ionization of Ni^{q+} ions (q = 10, 11, 13, 15). Experimental M-shell Ni^{9+}–Ni^{13+} spectra in the 14.4−16.5 nm region from the JET tokamak and from the reversed field pinch RFX have been recently simulated by Mattioli et al. [31]. However, there is a paucity of data available for electron impact excitation of Ni XI.

In the present work, we have used the Breit-Pauli R-matrix method as developed by Berrington et al. [32] and Scott and Burke [33], and also used successfully by various authors [34]. We have carried out fairly extensive relativistic R-matrix calculations to obtain electron impact excitation collision strengths and effective collision strengths for transitions from the ground state to the first 16 fine-structure levels of argon-like Ni XI. This method permits the explicit inclusion of the effect of resonances converging to all target states included in the calculation. The electron collision excitation processes that we specifically concentrate on in this paper are the following:

$$e^- + \mathrm{Ni}^{10+}\left(1s^2 2s^2 2p^6 3s^2 3p^6\ ^1\mathrm{S}^e\right) \rightarrow e^- + \mathrm{Ni}^{10+}\left(1s^2 2s^2 2p^6 3s^2 3p^5 3d\ ^3\mathrm{P}^\circ,\ ^3\mathrm{F}^\circ,\ ^1\mathrm{D}^\circ,\ ^3\mathrm{D}^\circ,\ ^1\mathrm{F}^\circ,\ ^1\mathrm{P}^\circ; 1s^2 2s^2 2p^6 3s 3p^6 3d\ ^3\mathrm{D}^e,\ ^1\mathrm{D}^e\right).$$

The target state wavefunctions are expressed in configuration interaction (CI) form and are determined using the code CIV3 [35]. The relativistic effects are incorporated in the Breit-Pauli approximation by including one-body mass correction, Darwin, and spin-orbit relativistic terms in the scattering equations. The collision strengths have been computed at a large number of electron incident energies and listed at selected values in the range 10 to 75 Rydberg. Finally, the effective collision strengths, obtained by averaging the collision strengths over a Maxwellian distribution for the velocity of the incident electron, are tabulated over a wide range of temperatures. These temperatures should cover the temperature of formation of Ni XI lines in various astrophysical plasmas.

2 Theoretical details

2.1 Target calculations

Accurate description of target wavefunctions is an essential component of any reliable scattering calculation. In the present scattering calculation on Ar-like Ni XI, the 9 lowest ionic states belonging to the $3s^2 3p^6$, $3s^2 3p^5 3d$, and $3s 3p^6 3d$ configurations are represented by restricted CI expansions, which include the most important configurations while keeping the scattering calculation tractable.

The wavefunctions are represented by expansions of the form

$$\Phi\ (LSJ) = \sum_{i=1}^{M} a_i\, \phi_i\,(\alpha_i,\ LSJ) \qquad (1)$$

where the single configuration functions $\{\Phi_i\}$ are constructed from one-electron orbitals, whose angular momenta are coupled as specified by $\{\alpha_i\}$ to form a total L and S common to all M configurations in equation (1). The radial part of each orbital is written as a linear combination of normalized Slater-type orbitals

$$P_{n\ell}\,(r) = \sum_{i=1}^{k} b_i \left(\frac{(2\zeta_i)^{2p_i+1}}{(2p_i)!}\right)^{\frac{1}{2}} r^{p_i} \exp(-\zeta_i\, r). \qquad (2)$$

The parameters $\{b_i\}$, $\{\zeta_i\}$ and $\{p_i\}$ in equation (2) and the mixing coefficients $\{a_i\}$ in equation (1) are determined variationally, as described by Hibbert [35]. In our calculations, we have used nine orthogonal one-electron orbitals: $1s$, $2s$, $2p$, $3s$, $3p$, $3d$, $4s$, $4p$, and $4d$. The first four are chosen as the Hartree-Fock orbitals for the ground $3p^5(^2\mathrm{P}^\circ)$ state of the chlorine-like Ni XII ion [36]. The $3p$ orbital is reoptimized on $3s^2 3p^5 4s$ ($^3\mathrm{P}^\circ$) of Ni XI by the exponents taken from the Hartree-Fock orbital of $3s^2 3p^5(^2\mathrm{P}^\circ)$ of Ni XII. The $3d$ and $4s$ functions are chosen as the spectroscopic type and are optimized on the excited states $3s^2 3p^5 3d$ ($^1\mathrm{D}^\circ$), and $3s^2 3p^5 4s$ ($^3\mathrm{P}^\circ$), respectively. The $4p$ orbital is chosen to give an accurate representation of $3s^2 3p^6 – 3s^2 3p^5 4p$ correlation effect in the lowest $^1\mathrm{S}$ state. The $4d$ orbital is optimized on the $3s^2 3p^5 3d\ ^1\mathrm{P}^\circ$ state, with configurations $3s^2 3p^5 3d$ and $3s^2 3p^5 4d$. The optimized radial function parameters of these orbitals are listed in Table 1. Table 2 gives the restricted list of configurations included in the scattering calculation to represent the nine states. In Table 3, we have compared our ab initio theoretical excitation energies (relative to the ground state) of the fine-structure levels of Ni XI, with the latest

Table 1. Values of parameters b_i, p_i and ζ_i for bound orbitals of Ni XI.

Orbital	Clementi coefficient (b_i)	Power of r (p_i)	Exponent (ζ_i)
$4s$	0.10670	1	20.17841
	–0.40318	2	9.98301
	1.03687	3	5.35956
	–1.38933	4	3.54278
$3p$	–0.36778	2	12.14670
	–0.03017	2	20.03440
	0.69282	3	5.97089
	0.45078	3	4.98200
	–0.12797	3	10.76050
$4p$	0.54869	2	11.35893
	–2.51553	3	5.25834
	2.59835	4	4.91387
$3d$	0.20453	3	9.00455
	0.84226	3	4.86896
$4d$	2.72301	3	8.07848
	0.02011	3	21.93487
	0.08643	4	9.33333
	–2.55681	4	8.06956

Table 2. Configurations used in the CI expansion of Ni XI target states.

Target states	State number	Configurations used
^{1}S	1	$[1s^2 2s^2 2p^6]$ $3s^2 3p^6$, $3s^2 3p^4 3d^2$
^{3}P°	2, 3, 4	$[1s^2 2s^2 2p^6]$ $3s^2 3p^5 3d$, $3s^2 3p^3 3d^3$, $3s 3p^5 3d^2$
^{3}F°	5, 6, 7	$[1s^2 2s^2 2p^6]$ $3s^2 3p^5 3d$, $3s^2 3p^3 3d^3$, $3s 3p^5 3d^2$
^{3}D°	8, 10, 11	$[1s^2 2s^2 2p^6]$ $3s^2 3p^5 3d$, $3s^2 3p^3 3d^3$, $3s 3p^5 3d^2$
^{1}D°	9	$[1s^2 2s^2 2p^6]$ $3s^2 3p^5 3d$, $3s^2 3p^3 3d^3$, $3s 3p^5 3d^2$
^{1}F°	12	$[1s^2 2s^2 2p^6]$ $3s^2 3p^5 3d$, $3s^2 3p^3 3d^3$
^{1}P°	13	$[1s^2 2s^2 2p^6]$ $3s^2 3p^5 3d$, $3s^2 3p^3 3d^3$
^{3}D	14, 15, 16	$[1s^2 2s^2 2p^6]$ $3s 3p^6 3d$, $3s 3p^4 3d^3$, $3s^2 3p^4 3d^2$
^{1}D	17	$[1s^2 2s^2 2p^6]$ $3s 3p^6 3d$, $3s 3p^4 3d^3$

Table 3. Excitation thresholds for Ni XI (in Rydberg).

Key	Configuration	State	J	Present results	NIST
1	$1s^2 2s^2 2p^6 3s^2 3p^6$	^{1}S	0	0.00000	0.0000
2	$1s^2 2s^2 2p^6 3s^2 3p^5 3d$	^{3}P°	0	4.34736	4.2766
3	$1s^2 2s^2 2p^6 3s^2 3p^5 3d$	^{3}P°	1	4.38366	4.3098
4	$1s^2 2s^2 2p^6 3s^2 3p^5 3d$	^{3}P°	2	4.45723	4.3811
5	$1s^2 2s^2 2p^6 3s^2 3p^5 3d$	^{3}F°	4	4.64639	4.4930
6	$1s^2 2s^2 2p^6 3s^2 3p^5 3d$	^{3}F°	3	4.68656	4.5285
7	$1s^2 2s^2 2p^6 3s^2 3p^5 3d$	^{3}F°	2	4.73636	-
8	$1s^2 2s^2 2p^6 3s^2 3p^5 3d$	^{3}D°	3	4.93579	4.8043
9	$1s^2 2s^2 2p^6 3s^2 3p^5 3d$	^{1}D°	2	4.97061	4.8301
10	$1s^2 2s^2 2p^6 3s^2 3p^5 3d$	^{3}D°	1	5.02599	4.8735
11	$1s^2 2s^2 2p^6 3s^2 3p^5 3d$	^{3}D°	2	5.04846	4.9123
12	$1s^2 2s^2 2p^6 3s^2 3p^5 3d$	^{1}F°	3	5.12673	4.9485
13	$1s^2 2s^2 2p^6 3s^2 3p^5 3d$	^{1}P°	1	6.41884	6.1405
14	$1s^2 2s^2 2p^6 3s 3p^6 3d$	^{3}D	1	7.85347	-
15	$1s^2 2s^2 2p^6 3s 3p^6 3d$	^{3}D	2	7.86852	-
16	$1s^2 2s^2 2p^6 3s 3p^6 3d$	^{3}D	3	7.89090	-
17	$1s^2 2s^2 2p^6 3s 3p^6 3d$	^{1}D	2	9.00447	-

available NIST energy table [37,38] to access the quality of the target wave functions. These excitation energies are calculated by using the target wave functions that are used in our scattering calculation. The present calculated energies are within 4% of the experimental values as compiled in the NIST. A good agreement indicates that our wavefunctions are of good quality to yield reliable collision strengths.

A further indication of the reliability of the present wavefunction representation can be found by examining the close conformity between the length and velocity oscillator strength values for the transitions between the target states. In Table 4, we present the length (f_l) and velocity (f_v) forms of the oscillator strengths obtained with our nine-state target wavefunctions. There is normally a good agreement between the length and velocity forms of the oscillator strengths. In our present calculation, the length and velocity values of the oscillator strength for the dipole-allowed $3s^2 3p^6\ ^1\mathrm{S} \rightarrow 3s^2 3p^5 3d\ ^1\mathrm{P}^\circ$ transition are 2.57 and 2.51, respectively. Fuhr et al. [39] and Fawcett et al. [40] listed the oscillator strength for the $3s^2 3p^6\ ^1\mathrm{S}_0 \rightarrow 3s^2 3p^5 3d\ ^1\mathrm{P}^\circ_1$ transition as 2.31 and 3.25, respectively. Excellent agreement is evident between the present length and velocity values with differences better than 3% for the above transition. Our result is in much better agreement with the compilation of Fuhr et al. [39] compared with the theoretical value of Fawcett et al. [40].

The excitation energies were adjusted before the diagonalization of the Hamiltonian matrix inside the R-matrix sphere [41]. The theoretical adjusted energies are used in the R-matrix STGH code to insure the correct positioning of resonances. This adjustment is necessary in order to obtain the correct excited-state thresholds and thus would allow for a direct comparison with experimental data in future. We have taken a limited number of configurations for doing manageable scattering calculation because of the computer memory limitations. However, one can calculate very accurate energies [42] by taking more correlations and corresponding large number of configurations.

Table 4. Oscillator strengths for allowed transitions among the lowest 9 states in Ni XI.

Transitions	Oscillator strengths	
	f_l	f_v
$1s^22s^22p^63s^23p^6\ {}^1\mathrm{S} \rightarrow 1s^22s^22p^63s^23p^53d\ {}^1\mathrm{P}^\circ$	$0.25749 \times 10^{+1}$	$0.25069 \times 10^{+1}$
$1s^22s^22p^63s^23p^53d\ {}^3\mathrm{P}^\circ \rightarrow 1s^22s^22p^63s3p^63d\ {}^3\mathrm{D}$	0.73569×10^{-1}	0.79562×10^{-1}
$1s^22s^22p^63s^23p^53d\ {}^3\mathrm{F}^\circ \rightarrow 1s^22s^22p^63s3p^63d\ {}^3\mathrm{D}$	0.35929×10^{-1}	0.30645×10^{-1}
$1s^22s^22p^63s^23p^53d\ {}^3\mathrm{D}^\circ \rightarrow 1s^22s^22p^63s3p^63d\ {}^3\mathrm{D}$	0.24403×10^{-1}	0.22430×10^{-1}
$1s^22s^22p^63s^23p^53d\ {}^1\mathrm{D}^\circ \rightarrow 1s^22s^22p^63s3p^63d\ {}^1\mathrm{D}$	0.15859	0.14314
$1s^22s^22p^63s^23p^53d\ {}^1\mathrm{F}^\circ \rightarrow 1s^22s^22p^63s3p^63d\ {}^1\mathrm{D}$	0.18158	0.11642
$1s^22s^22p^63s^23p^53d\ {}^1\mathrm{P}^\circ \rightarrow 1s^22s^22p^63s3p^63d\ {}^1\mathrm{D}$	0.11359	0.17717

2.2 Scattering calculations

The total wave function for Ni XI plus electron system is expanded in an inner region ($r \leq a$) on a discrete basis of R-matrix states as [43]

$$\psi_k = A \sum_{i\,j} c_{ijk} \Phi_i \left(X_1 X_2 ... X_N;\, \hat{r}_{N+1},\, \sigma_{N+1}\right) u_{ij}\left(r_{N+1}\right) + \sum_j d_{jk}\, \phi_j (X_1 ... X_{N+1}) \quad (3)$$

where A is the antisymmetrization operator which accounts for electron exchange, and $\{\Phi_i\}$ are channel functions representing the 17 fine-structure target levels formed by coupling the target states of coordinates $X_i = \{r_i,\, \hat{r}_i,\, \sigma_i\}$ with the spin angle function of the scattered electron. The $\{u_{ij}\}$ form a discrete R-matrix basis of continuum orbitals for the scattered electron and the ϕ_j are $(N+1)$ electron bound configurations, which account for the orthogonality of the continuum orbitals u_{ij} to the bound orbitals and eventually for additional short-range correlation effects.

The continuum orbitals u_{ij} in equation (3) are solutions of the zero-order radial differential equation

$$\left(-d^2/dr^2 + l_i(l_i+1)/r^2 + 2V(r) - k_i^2\right) u_{ij}(r) = \sum \lambda_{ijk} P_k\left(r\right) \quad (4)$$

which satisfy the boundary conditions

$$u_{ij}(0) = 0, \quad (5)$$

$$\frac{a}{u_{ij}} \frac{du_{ij}}{dr}\Big|_{r\,=\,a} = b. \quad (6)$$

In equation (4), l_i is the angular momentum of the scattered electron; $V(r)$ is the static potential of the target in its ground state and $\{\lambda_{ijk}\}$ are Lagrange multipliers which are determined by imposing the orthogonality of the continuum orbitals to the bound radial orbitals $P_k(r)$ with the same angular momentum l_i. We have imposed a zero logarithmic derivative ($b = 0$ in Eq. (6)) on the continuum orbitals at the R-matrix boundary radius $a = 4$ a.u., and retained 12 continuum orbitals for each angular symmetry, to ensure convergence in the energy range considered here (up to 75 Ryd). The coefficients c_{ijk} and d_{jk} in equation (3) are determined by diagonalizing the $(N+1)$ electron Breit-Pauli Hamiltonian in the inner region.

In the outer region ($r > a$), it is important to take account of long-range coupling between the channels. The resulting coupled equations are solved using a perturbation method developed by Seaton [44] to yield K matrix and then the collision strengths. In our calculations, we have considered all partial waves up to $L = 9$ for both parities and spin multiplicities (doublets and quartets). These partial waves are sufficient to give converged results up to the highest energy for all the spin-changing transitions here.

3 Results and discussion

In Table 5, we list our collision strengths (Ω) for 16 transitions involving the 9 lowest states, at selected energy points. These energies are above the highest excitation threshold where resonances do not occur. The keys of the lower and upper levels involved in a transition are given in Table 3. As shown in Table 5, the $3s^23p^6\ {}^1\mathrm{S}_0 \rightarrow 3s^23p^53d\ {}^1\mathrm{P}^\circ_1$ transition has the largest collision strength as it is a dipole-allowed transition and corresponds to the excitation of electron from $3p$ state to $3d$ state. For the $3s^23p^6\ {}^1\mathrm{S}_0 \rightarrow 3s^23p^53d$ transitions, the lowest collision strength corresponds to the $3s^23p^6\ {}^1\mathrm{S}_0 \rightarrow 3s^23p^53d\ {}^3\mathrm{P}^\circ_0$ transition. Among the $3s^23p^6\ {}^1\mathrm{S}_0 \rightarrow 3s3p^63d$ transitions, the value of collision strength is the lowest for the $3s^23p^6\ {}^1\mathrm{S}_0 \rightarrow 3s3p^63d\ {}^3\mathrm{D}_1$ transition. Discussion of the present results poses some problems because there are no available calculations to our knowledge for collision strengths in Ni XI.

We show the variation of collision strength with incident electron energy in Figures 1, 2 and 3. We chose a fine energy mesh for collision strengths in the threshold energy region to resolve the dominant resonance structure. Figure 1 illustrates the results for the excitation from the ground state $3s^23p^6\ {}^1\mathrm{S}_0$ to the excited state $3s^23p^53d\ {}^1\mathrm{P}^\circ_1$. It clearly shows that, at low energies, the collision strengths are dominated by closed-channel (or Feshbach) resonances. Figures 2 and 3 display resonant collision strengths for the forbidden transitions, $3s^23p^6\ {}^1\mathrm{S}_0 \rightarrow 3s^23p^53d\ {}^3\mathrm{P}^\circ_0$ and $3s^23p^6\ {}^1\mathrm{S}_0 \rightarrow 3s3p^63d\ {}^3\mathrm{D}_1$, respectively, over the energy region from threshold to 20 Rydberg. The complicated resonance

Table 5. Collision strengths for electron excitation of Ni XI.

Transition (i, j)	Energy (Rydberg)									
	10	11	12	13	14	15	30	45	60	75
1-2	0.00314	0.00292	0.00273	0.00255	0.00239	0.00223	0.00083	0.00074	0.00034	0.00021
1-3	0.00988	0.00919	0.00858	0.00802	0.00751	0.00701	0.00254	0.00223	0.00100	0.00060
1-4	0.01746	0.01626	0.01518	0.01419	0.01326	0.01238	0.00420	0.00350	0.00141	0.00080
1-5	0.02202	0.02045	0.01903	0.01772	0.01650	0.01535	0.00491	0.00418	0.00160	0.00090
1-6	0.01694	0.01581	0.01479	0.01386	0.01298	0.01215	0.00453	0.00375	0.00178	0.00112
1-7	0.01061	0.00988	0.00922	0.00862	0.00805	0.00752	0.00266	0.00229	0.00101	0.00059
1-8	0.00704	0.00662	0.00625	0.00592	0.00561	0.00534	0.00316	0.00281	0.00225	0.00192
1-9	0.00594	0.00548	0.00507	0.00470	0.00436	0.00404	0.00132	0.00111	0.00048	0.00027
1-10	0.00424	0.00403	0.00384	0.00365	0.00345	0.00326	0.00166	0.00132	0.00085	0.00063
1-11	0.00499	0.00458	0.00422	0.00389	0.00359	0.00331	0.00093	0.00088	0.00030	0.00016
1-12	0.00835	0.00812	0.00794	0.00779	0.00767	0.00757	0.00705	0.00624	0.00600	0.00533
1-13	0.44704	0.45192	0.45910	0.46207	0.45784	0.44809	0.34297	0.25228	0.20428	0.16210
1-14	0.00487	0.00459	0.00432	0.00406	0.00381	0.00357	0.00135	0.00066	0.00036	0.00021
1-15	0.00769	0.00725	0.00683	0.00644	0.00605	0.00567	0.00217	0.00107	0.00059	0.00036
1-16	0.00993	0.00939	0.00887	0.00837	0.00789	0.00741	0.00289	0.00144	0.00079	0.00049
1-17	0.02791	0.02827	0.02877	0.02932	0.02980	0.03015	0.03269	0.03351	0.03208	0.03064

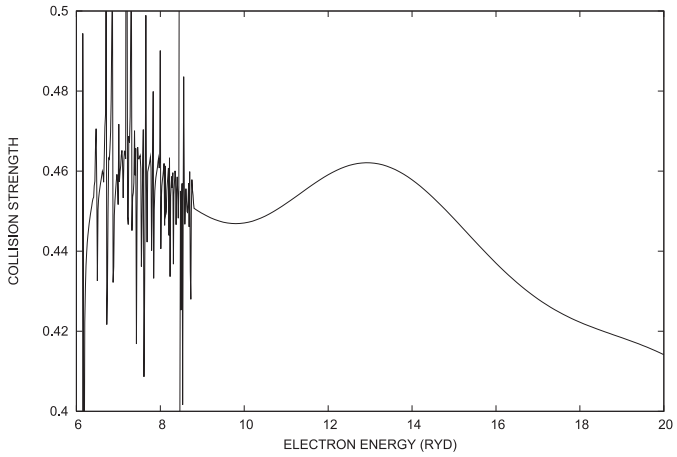

Fig. 1. Collision strength for $3s^2 3p^6\ {}^1\mathrm{S}_0 \rightarrow 3s^2 3p^5 3d\ {}^1\mathrm{P}_1^\circ$ (1-13) in Ni XI, as a function of incident electron energy in Rydbergs.

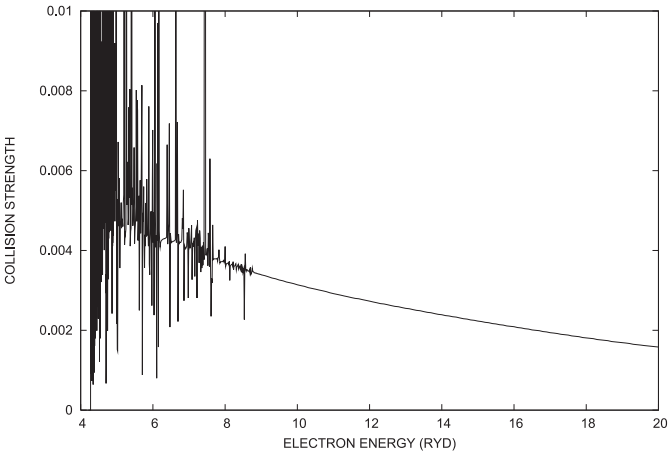

Fig. 2. Collision strength for $3s^2 3p^6\ {}^1\mathrm{S}_0 \rightarrow 3s^2 3p^5 3d\ {}^3\mathrm{P}_0^\circ$ (1-2) in Ni XI, as a function of incident electron energy in Rydbergs.

structures due to the Rydberg series converging to the various excited level thresholds can be clearly seen in these figures. The background collision strength away from the resonances is small for the forbidden transitions, and the contribution from the resonances dominate the collision strengths.

For many astrophysical and plasma applications, it is the fine structure rate coefficient which is needed rather than the energy dependent collision strength. The effective collision strengths are calculated by taking into account important resonance structures. We have integrated resonant collision strengths below the highest excitation threshold and the smooth collision strengths above the highest threshold over a Maxwellian distribution of electron energies. The excitation rate coefficient for a transition from state i to state f at electron temperature T_e is

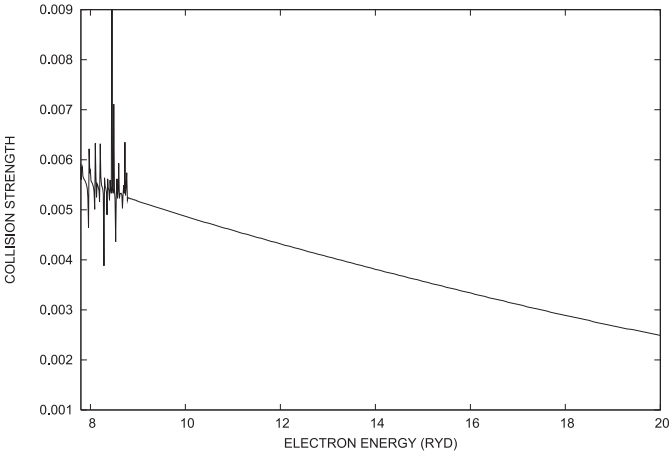

Fig. 3. Collision strength for $3s^2 3p^6\ {}^1\mathrm{S}_0 \rightarrow 3s3p^6 3d\ {}^3\mathrm{D}_1$ (1-14) in Ni XI, as a function of incident electron energy in Rydbergs.

Table 6. Effective collision strengths for transitions in Ni XI.

Transition	Temperature (10^4 K)							
(i,j)	2	3	4	6	8	10	20	40
	60	80	100	200	400	600	800	1000
1-2	1.780×10^{-2}	1.557×10^{-2}	1.413×10^{-2}	1.235×10^{-2}	1.124×10^{-2}	1.045×10^{-2}	8.309×10^{-3}	6.491×10^{-3}
	5.544×10^{-3}	4.920×10^{-3}	4.464×10^{-3}	3.226×10^{-3}	2.239×10^{-3}	1.759×10^{-3}	1.464×10^{-3}	1.263×10^{-3}
1-3	4.970×10^{-2}	4.487×10^{-2}	4.153×10^{-2}	3.712×10^{-2}	3.421×10^{-2}	3.207×10^{-2}	2.587×10^{-2}	2.031×10^{-2}
	1.736×10^{-2}	1.541×10^{-2}	1.398×10^{-2}	1.011×10^{-2}	7.004×10^{-3}	5.475×10^{-3}	4.523×10^{-3}	3.864×10^{-3}
1-4	8.260×10^{-2}	7.364×10^{-2}	6.753×10^{-2}	5.962×10^{-2}	5.455×10^{-2}	5.090×10^{-2}	4.089×10^{-2}	3.246×10^{-2}
	2.805×10^{-2}	2.511×10^{-2}	2.293×10^{-2}	1.701×10^{-2}	1.214×10^{-2}	9.602×10^{-3}	7.976×10^{-3}	6.836×10^{-3}
1-5	1.001×10^{-1}	9.064×10^{-2}	8.493×10^{-2}	7.780×10^{-2}	7.292×10^{-2}	6.904×10^{-2}	5.636×10^{-2}	4.405×10^{-2}
	3.754×10^{-2}	3.325×10^{-2}	3.012×10^{-2}	2.156×10^{-2}	1.470×10^{-2}	1.137×10^{-2}	9.313×10^{-3}	7.909×10^{-3}
1-6	8.522×10^{-2}	8.154×10^{-2}	7.796×10^{-2}	7.210×10^{-2}	6.752×10^{-2}	6.375×10^{-2}	5.132×10^{-2}	3.927×10^{-2}
	3.297×10^{-2}	2.892×10^{-2}	2.604×10^{-2}	1.855×10^{-2}	1.287×10^{-2}	1.010×10^{-2}	8.376×10^{-3}	7.184×10^{-3}
1-7	6.087×10^{-2}	5.672×10^{-2}	5.311×10^{-2}	4.775×10^{-2}	4.394×10^{-2}	4.104×10^{-2}	3.240×10^{-2}	2.466×10^{-2}
	2.069×10^{-2}	1.813×10^{-2}	1.630×10^{-2}	1.155×10^{-2}	7.944×10^{-3}	6.203×10^{-3}	5.125×10^{-3}	4.385×10^{-3}
1-8	5.514×10^{-2}	4.884×10^{-2}	4.456×10^{-2}	3.893×10^{-2}	3.526×10^{-2}	3.260×10^{-2}	2.521×10^{-2}	1.888×10^{-2}
	1.569×10^{-2}	1.368×10^{-2}	1.229×10^{-2}	8.908×10^{-3}	6.576×10^{-3}	5.460×10^{-3}	4.747×10^{-3}	4.237×10^{-3}
1-9	3.239×10^{-2}	3.355×10^{-2}	3.348×10^{-2}	3.217×10^{-2}	3.052×10^{-2}	2.895×10^{-2}	2.333×10^{-2}	1.759×10^{-2}
	1.450×10^{-2}	1.250×10^{-2}	1.109×10^{-2}	7.561×10^{-3}	5.077×10^{-3}	3.936×10^{-3}	3.250×10^{-3}	2.787×10^{-3}
1-10	1.276×10^{-2}	1.273×10^{-2}	1.262×10^{-2}	1.226×10^{-2}	1.184×10^{-2}	1.144×10^{-2}	9.847×10^{-3}	8.012×10^{-3}
	6.960×10^{-3}	6.257×10^{-3}	5.748×10^{-3}	4.436×10^{-3}	3.389×10^{-3}	2.821×10^{-3}	2.450×10^{-3}	2.187×10^{-3}
1-11	2.235×10^{-2}	2.229×10^{-2}	2.174×10^{-2}	2.042×10^{-2}	1.921×10^{-2}	1.818×10^{-2}	1.480×10^{-2}	1.146×10^{-2}
	9.638×10^{-3}	8.433×10^{-3}	7.567×10^{-3}	5.354×10^{-3}	3.719×10^{-3}	2.919×10^{-3}	2.419×10^{-3}	2.075×10^{-3}
1-12	9.296×10^{-2}	8.371×10^{-2}	7.805×10^{-2}	7.036×10^{-2}	6.467×10^{-2}	6.010×10^{-2}	4.572×10^{-2}	3.270×10^{-2}
	2.637×10^{-2}	2.259×10^{-2}	2.008×10^{-2}	1.441×10^{-2}	1.103×10^{-2}	9.668×10^{-3}	8.914×10^{-3}	8.417×10^{-3}
1-13	4.217×10^{-1}	4.311×10^{-1}	4.369×10^{-1}	4.438×10^{-1}	4.476×10^{-1}	4.498×10^{-1}	4.534×10^{-1}	4.533×10^{-1}
	4.508×10^{-1}	4.467×10^{-1}	4.415×10^{-1}	4.104×10^{-1}	3.546×10^{-1}	3.144×10^{-1}	2.848×10^{-1}	2.619×10^{-1}
1-14	6.305×10^{-3}	6.053×10^{-3}	5.922×10^{-3}	5.777×10^{-3}	5.684×10^{-3}	5.612×10^{-3}	5.341×10^{-3}	4.936×10^{-3}
	4.600×10^{-3}	4.310×10^{-3}	4.055×10^{-3}	3.143×10^{-3}	2.197×10^{-3}	1.705×10^{-3}	1.402×10^{-3}	1.196×10^{-3}
1-15	9.771×10^{-3}	9.443×10^{-3}	9.265×10^{-3}	9.058×10^{-3}	8.922×10^{-3}	8.812×10^{-3}	8.399×10^{-3}	7.774×10^{-3}
	7.254×10^{-3}	6.802×10^{-3}	6.404×10^{-3}	4.977×10^{-3}	3.487×10^{-3}	2.706×10^{-3}	2.220×10^{-3}	1.886×10^{-3}
1-16	1.104×10^{-2}	1.112×10^{-2}	1.114×10^{-2}	1.113×10^{-2}	1.108×10^{-2}	1.101×10^{-2}	1.065×10^{-2}	9.943×10^{-3}
	9.316×10^{-3}	8.757×10^{-3}	8.260×10^{-3}	6.453×10^{-3}	4.541×10^{-3}	3.528×10^{-3}	2.893×10^{-3}	2.454×10^{-3}
1-17	2.922×10^{-2}	2.872×10^{-2}	2.845×10^{-2}	2.820×10^{-2}	2.810×10^{-2}	2.806×10^{-2}	2.813×10^{-2}	2.855×10^{-2}
	2.896×10^{-2}	2.931×10^{-2}	2.960×10^{-2}	3.056×10^{-2}	3.106×10^{-2}	3.079×10^{-2}	3.023×10^{-2}	2.951×10^{-2}

given by Eissner and Seaton [45]

$$C\,(i\rightarrow f) = \frac{8.6287\times10^{-6}}{g_i T^{1/2}}\gamma(i\rightarrow f) \times \exp\left(-\frac{\Delta E_{if}}{kT}\right)\ \mathrm{cm^3\,s^{-1}} \quad (7)$$

where $g_i = (2j_i + 1)$ is the statistical weight of the lower level i, $\Delta E_{if} = E_f - E_i$ is the excitation energy, and $\gamma(i \rightarrow f)$ is the dimensionless quantity called effective collision strength defined as

$$\gamma(i\rightarrow f) = \int_0^\infty \Omega(i\rightarrow f)\exp(-\varepsilon_f/kT)d(\varepsilon_f/kT) \quad (8)$$

where $\Omega(i \rightarrow f)$ is the total collision strength for transitions between levels i and f, k is the Boltzmann constant, and ε_f is the energy of the incident electron with respect to the upper level f, and T_e is the electron temperature. In Table 6, we have listed the effective collision strengths $\gamma\,(i \rightarrow f)$ for transitions between the ground state and 16 excited levels belonging to the $3p^5 3d$ and $3s3p^6 3d$ configurations. The keys to the levels of transitions are given in Table 3. The values of effective collision strengths are larger for the dipole-allowed transition $3s^2 3p^6\ {}^1\mathrm{S}_0 \rightarrow 3s^2 3p^5 3d\ {}^1\mathrm{P}^\circ_1$ as compared to the spin-forbidden transitions. We are not aware of other published results for this ion to compare with our calculations. However, we have calculated the effective collision strengths over a wide temperature range (2×10^4–1×10^7 K), which is of interest to astrophysics.

4 Conclusions

In conclusion, we presented elaborate calculations of collision strengths and effective collision strengths for transitions between the ground state and levels of $3s^2 3p^5 3d$ and $3s3p^6 3d$ configurations using the relativistic Breit-Pauli R-matrix method. The contributions of resonances converging to the different excited levels are included in the collision strengths for the fine-structure transitions. The effective collision strengths are presented over a wide range of electron temperatures suitable for use in plasma modelling. Theoretical calculations of electron impact excitation processes in atomic ions have important applications in high temperature plasma research. Of particular importance are studies of transition metal ions, such as Ni, which are directly applicable to plasma cooling, transport, and confinement in experimental fusion devices. We expect our results to be quite reliable, as we have taken all the important physical effects like exchange, channel coupling, short-range correlation and relativistic effects into account. These are the first detailed calculations of collision strength and effective collision strength for Ni XI. This will help redress the present scarcity of data in this field.

M.M. is thankful to DST (India) and UGC (India) for financial support. A.K.S.J. is thankful to DST for junior research fellow.

References

1. R.K. Javev, Phys. Scripta **T37**, 5 (1991)
2. U. Feldman, W. Curdlt, E. Landi, K. Wilhelm, ApJ **544**, 508 (2000)
3. H.P. Warren, ApJS **157**, 147 (2005)
4. M. Kretzschmar, J. Lilensten, J. Aboudarham, A&A **419**, 345 (2004)
5. D.L. Garrett, R. Tousey, Appl. Opt. **16**, 898 (1977)
6. M. Malinovsky, L. Heroux, ApJ **181**, 1009 (1973)
7. G.M. Nikolsky, Sol. Phys. **6**, 399 (1969)
8. Z.-X. Shen, B. Jones, D.N.C. Lin, X.-W. Liu, S.-L. Li, ApJ **635**, 608 (2005)
9. A.J.J. Raassen, R. Mewe, M. Audard, M. Güdel, E. Behar, J.S. Kaastra, R.L.J. van der Meer, C.R. Foley, J.U. Ness, A&A **389**, 228 (2002)
10. A.J.J. Raassen, J.U. Ness, R. Mewe, R.L.J. van der Meer, V. Burwitz, J.S. Kaastra, A&A **400**, 671 (2003)
11. N. Craig, M. Abbott, D. Finley, H. Jessop, S.B. Howell, M. Mathioudakis, J. Sommers, J.V. Vallerga, R.F. Malina, ApJS **113**, 131 (1997)
12. K.P. Dere, H.E. Mason, K.G. Widing, A.K. Bhatia, ApJS **40**, 341 (1979)
13. A.K. Bhatia, E. Landi, W. Eissner, At. Data Nucl. Data Tables **92**, 105 (2006)
14. J.L. Linsky, private communication (1991)
15. U. Feldman, B.S. Fraenkel, S. Hoory, ApJ **142**, 719 (1965)
16. H.E. Hinteregger, L.A. Hall, W. Schweitzer, ApJ **140**, 319 (1964)
17. E. Alexander, U. Feldman, B.S. Fraenkel, S. Hoory, Nature **206**, 176 (1965)
18. A.H. Gabriel, B.C. Fawcett, C. Jordan, Proc. Phys. Soc. **87**, 825 (1966)
19. W.J. Wagner, L.L. House, ApJ **166**, 683 (1971)
20. L.A. Svensson, J.O. Ekberg, B. Edlén, Sol. Phys. **34**, 173 (1974)
21. W.E. Behring, L. Cohen, U. Feldman, G.A. Doschek, ApJ **203**, 521 (1976)
22. M. Even-Zohar, B.S. Fraenkel, J. Opt. Soc. Am. **58**, 1420 (1968)
23. B. Edlén, R. Smitt, Sol. Phys. **57**, 329 (1978)
24. G.D. Sandlin, R. Tousey, ApJ **227**, L107 (1979)
25. A. Alexander, U. Feldman, B.S. Fraenkel, J. Opt. Soc. Am. **55**, 650 (1965)
26. B.C. Fawcett, R.D. Cowan, R.W. Hayes, J. Phys. B: At. Mol. Opt. Phys. **5**, 2143 (1972)
27. F. Magnant-Crifo, Sol. Phys. **41**, 109 (1975)
28. D.C. Griffin, M.S. Pindzola, J. Phys. B: At. Mol. Opt. Phys. **21**, 3253 (1988)
29. L.J. Wang, K. Rinn, D.C. Gregory, J. Phys. B: At. Mol. Opt. Phys. **21**, 2117 (1988)
30. S. Cherkani-Hassani, M. Khouilid, P. Defrance, Phys. Scripta **T92**, 287 (2001)
31. M. Mattioli, K.B. Fournier, I. Coffey, M. Finkenthal, C. Jupén, M. Valisa, J. Phys. B: At. Mol. Opt. Phys. **37**, 13 (2004)
32. K.A. Berrington, W.B. Eissner, P.H. Norrington, Comput. Phys. Commun. **92**, 290 (1995)
33. N.S. Scott, P.G. Burke, J. Phys. B: At. Mol. Opt. Phys. **13**, 4299 (1980)
34. M. Mohan, A.K.S. Jha, N. Singh, Phys. Scripta **73**, 601 (2006); A.K.S. Jha, P. Jha, S. Tyagi, M. Mohan, Eur. Phys. J. D **39**, 391 (2006); A.K.S. Jha, N. Singh, N. Verma, M. Mohan, Can. J. Phys. **84**, 707 (2006)
35. A. Hibbert, Comput. Phys. Commun. **9**, 141 (1975)
36. E. Clementi, C. Roetti, At. Data Nucl. Data Tables **14**, 177 (1974)
37. NIST Atomic Spectra Database website `http://physics.nist.gov/cgi-bin/AtData/Level_form`
38. J. Sugar, C. Corliss, J. Phys. Chem. Ref. Data **14**, 664 (1985)
39. J.R. Fuhr., G.A. Martin, W.L. Wiese, J. Phys. Chem. Ref. Data **17**, 504 (1988)
40. B.C. Fawcett, N.J. Peacock, R.D. Cowan, J. Phys. B: At. Mol. Opt. Phys. **1**, 295 (1968)
41. K. Bartschat, B.M. McLaughlin, R.A. Hoversten, J. Phys. B: At. Mol. Opt. Phys. **24**, 3359 (1991)
42. N. Verma, A.K.S. Jha, M. Mohan, J. Phys. B **38**, 3185 (2005); N. Verma, A.K.S. Jha, M. Mohan, ApJS **164**, 297 (2006)
43. P.G. Burke, W.D. Robb, Adv. At. Mol. Phys. **11**, 143 (1975)
44. M.J. Seaton, J. Phys. B: At. Mol. Opt. Phys. **18**, 2111 (1985)
45. W. Eissner, M.J. Seaton, J. Phys. B: At. Mol. Opt. Phys. **7**, 2533 (1974)